Institute for Computational Mathematics
Hong Kong Baptist University

ICM Research Report
09-09

A MULTIPHASE IMAGE SEGMENTATION METHOD BASED ON FUZZY REGION COMPETITION *

FANG LI †, MICHAEL K. NG ‡, TIE YONG ZENG §, AND CHUNLI SHEN¶

Abstract. The goal of this paper is to develop a multiphase image segmentation method based on fuzzy region competition. A new variational functional with constraints is proposed by introducing fuzzy membership functions which represent several different regions in an image. The existence and symmetry of minimizer of this functional are established. In order to handle the constraints of membership functions in the minimization, we propose three methods incorporating Karush-Kuhn-Tucker (KKT) conditions. We also add auxiliary variables to approximate the membership functions in the functional such that Chambolle's fast dual projection method can be used. An alternate minimization method can be employed to find the solution, in which the region parameters and the membership functions have closed form solutions. Numerical examples on gray scale and color images are given to demonstrate the effectiveness of the proposed methods.

Keywords: multiphase, image segmentation, region competition, fuzzy membership function, alternative minimization.

1. Introduction. Image segmentation plays a very important role in computer vision. The aim is to partition an image into several regions so that each region has uniform characteristics like edges, intensities, color and texture etc. In the past decades, this problem has been extensively studied by variational methods and partial differential equations (PDE). The snake model [13], geodesic active contour model [4] use edge detection functions and evolve the curve towards sharp gradient. However, the edge based method is not robust to noise, and generally a noisy image has to be smoothed. Region based methods incorporate region and boundary information and are robust to noise. One of the most well known region based method is the Mumford-Shah model [18], which approximates an image by piecewise smooth function with regular boundaries. The difficulty in studying the Mumford-Shah functional is that it involves two unknowns: the intensity function and the set of edges. The Mumford-Shah model is hard to implement in practice since the discretization of the unknown set of edges is a very complex task. A commonly used method is to approximate the Mumford-Shah functional by a sequence of regular functionals defined on Sobolev spaces, which converges to Mumford-Shah functional in the sense of Γ-convergence [1]. In the regular functionals, the set of edges does not appear. The special case of piecewise constant Mumford-Shah model is studied by Chan et al [5, 6] using level set method [21]. Zhu et al [22] proposed a region competition method by unifying snake, region growing and Bayesian statistics. This method penalizes the length of the boundaries and the Bayesian error within each region. The error is estimated by parametric probability distributions such as Gaussian distribution. Then piecewise constant Mumford-Shah model can be regarded as a special case of region competition method. Curve evolution techniques are used in the implementation of region competition.

*Research supported in part by RGC 201508, HKBU FRGs, and The Research Fund for the Doctoral Program of Higher Education (200802691037).

†Department of Mathematics, East China Normal University, Shanghai, China

‡The Corresponding Author, Centre for Mathematical Imaging and Vision, and Department of Mathematics, Hong Kong Baptist University, Kowloon Tong, Hong Kong. E-mail: mng@math.hkbu.edu.hk.

§Department of Mathematics, Hong Kong Baptist University, Kowloon Tong, Hong Kong.

¶Department of Mathematics, East China Normal University, Shanghai, China

Multiphase segmentation is a more challenge problem than two-phase segmentation. The main difficulty is to find effective representations of the regions and their boundaries. There are several recent works related to the multiphase Mumford-Shah model. Vese et al [23] generalized the two-phase model [5] to multiphase segmentation by using multi level set functions. Both piecewise constant and piecewise smooth cases are studied. The advantage of using level set functions to represent the regions is that it automatically avoids the problems of vacuum and overlap. However, this method has several disadvantages: (i) The numerical solution of the level set equation is obtained by gradient descent method which converges slowly and is easy to trap into local minima. (ii) For numerical stability, the level set function should be reinitialized as sign distance function periodically. (iii) Multiple regions cannot be handled in a straight-forward manner. The evolution equation of the level set functions can hardly be unified such that one must write down the equation for each level set, which is a tedious task.

Samson et al [20] proposed another level set based multiphase segmentation model by adding a penalty term of the level set functions to penalize the vacuum and overlap. We note that their idea inspires our proposed method in dealing with the summation to one constraint of membership functions. In this formulation, the multiple region can be handled directly. However, the numerical disadvantages of local minima and reinitialization of level set function are still remained. Lie et al [15] proposed to use binary level set functions which takes value 1 or -1 instead of the classical continuous level set functions in the piecewise constant Mumford-Shah segmentation framework. A smooth convex functional with a quadratic constraint is minimized and no reinitialization of level set function is needed. Then, Lie at al [16] introduced a piecewise constant level set function and use each constant value to represent a unique phase in piecewise constant segmentation model. Their approach has difficulties in representing the unit normal and the mean curvature for the curves, which is easily done by classical level set. Another disadvantage of their method is the sensitivity to initial guess. Jung et al [12] proposed a phase field method to handle multiphase piecewise constant segmentation. The method is based on the phase transition model of Modica and Mortola with a sinusoidal potential. Since the model is not quadratic or convex, a convex-concave procedure is used in the implementation. The Γ-convergence behavior of their model and the existence of its minimizers are established. Chung et al [9] proposed a multilayer approach for multiphase piecewise constant segmentation. In the method, several level lines of the same level set function are used to represent the boundaries of regions, which have the property that one region is subset to another. It takes almost one page to write down the evolution equation of two level set functions with m and n layers respectively.

Different from the above mentioned methods which yields hard segmentation result, fuzzy segmentation approaches are popular in data mining and medical image segmentation [2]. In the fuzzy method, it is assumed that each image pixel can be associated in several regions. The probability is represented by fuzzy membership functions valued in [0,1]. Recently, many two-phase fuzzy segmentation models are proposed [7, 3, 17, 10], in which one fuzzy membership function is used in the functionals such that the functionals are convex with respect to the membership. The convexity ensures that the new methods are not sensitive to initialization and global minima can be possibly found. Another advantage is that Chambolle's fast dual projection method [8] can be adopted in the implementation. However, this technique is used only in two-phase segmentation. Extension of this framework to multi-phase

segmentation is not trivial. A general multiphase stochastic variational soft segmentation model was proposed by Shen [24] based on the Mumford-Shah model. Shen used stochastic variables (as fuzzy membership functions) to represent the ownership of each class, which are regularized by a regularization term with a double well potential related to phase field. However, the energy functional in this model is nonconvex with respect to each stochastic variable. Moreover, a set of PDEs of the stochastic variables have to be solved, which makes the implementation computationally expensive.

In this paper, we develop and study a multiphase image segmentation method based on fuzzy region competition. The new variational functional is obtained by introducing fuzzy membership functions in the original region competition functional. The existence and symmetry of minimizer of this new functional are established. We need to minimize the functional under two convex constraints of membership functions. Three methods coupled with Karush-Kuhn-Tucker conditions are proposed to handle the constraints in the minimization procedure. We also add auxiliary variables to approximate the membership functions in the functional such that Chambolle's fast dual projection method can be used, meanwhile, the membership functions have closed form solutions. An alternate minimization method can be employed to find the solution of the problem. Numerical examples on gray scale and color images are given to demonstrate the promising results of the proposed methods.

The outline of this paper is as follows. In Section 2, we review related works. In Section 3, we propose and analyze our model. In Section 4, we present our algorithm. In Section 5, an extension to vector-valued images is considered. In Section 6, experimental results are presented to illustrate the effectiveness of our model. Concluding remarks are given in Section 7.

2. Related Works. The segmentation problem can be formulated as follows: Given a gray scale image $I : \Omega \to \mathbb{R}$ where the image domain Ω is a bounded, smooth and open subset of $\mathbb{R}^2$, the aim is to partition Ω into N regions $\{\Omega_i\}_{i=1}^N$ such that $\Omega_i \bigcap \Omega_j = \emptyset, j \neq i$ and $\bigcup_{i=1}^N \Omega_i = \Omega$ by certain suitable measure.

2.1. Mumford-Shah model. Mumford and Shah [18] proposed to solve the segmentation problem by minimizing the following energy

$$E_{MS}(g,\Gamma) = \lambda \int_\Omega (I-g)^2 dx + \mu \int_{\Omega-\Gamma} |\nabla g|^2 dx + |\Gamma| \tag{2.1}$$

where $\Gamma = \bigcup \partial\Omega_i$ is the union of boundaries of Ω_i, $|\Gamma|$ denotes the arc length of curve Γ, λ, μ are the weight parameters. The interpretation of the three terms is as follows: the first term requires that g approximates I; the second term requires that g does not vary very much on each Ω_i; the third term requires that the boundary Γ be as short as possible. Here g is a piecewise smooth approximate function of image I. In particular, Mumford and Shah considered the special case where the function g is chosen to be a piecewise constant function.

2.2. Chan-Vese model. The piecewise constant Mumford-Shah model is studied by Chan et al using the level set method [5, 6, 23]. Chan and Vese [5] proposed the following minimization method for two-phase segmentation:

$$\min \left\{ E_{CV}(\Gamma, c_1, c_2) = \mu|\Gamma| + \lambda_1 \int_{inside(\Gamma)} |I-c_1|^2 dx + \lambda_2 \int_{outside(\Gamma)} |I-c_2|^2 dx \right\}.$$

In the level set method [21], $\Gamma \subset \Omega$ is represented by the zero level set of a Lipschitz function $\phi : \Omega \to \mathbb{R}$, such that

$$\begin{cases} \Gamma = \{x \in \Omega : \phi(x) = 0\}, \\ inside(\Gamma) = \{x \in \Omega : \phi(x) > 0\}, \\ outside(\Gamma) = \{x \in \Omega : \phi(x) < 0\}. \end{cases}$$

Then the level set formulation of Chan-Vese model is

$$\min \left\{ \begin{array}{c} E_{CV}(\phi, c_1, c_2) = \mu \int_\Omega |\nabla H(\phi)|\, dx \ + \lambda_1 \int_\Omega |u_0 - c_1|^2 H(\phi) dx \\ +\lambda_2 \int_\Omega |u_0 - c_2|^2 (1 - H(\phi))\, dx \end{array} \right\}. \tag{2.2}$$

where $H(\phi)$ is the Heaviside function: $H(\phi) = 1$ if $\phi \geq 0$ and $H(\phi) = 0$ otherwise. The evolution equation of ϕ is

$$\frac{\partial \phi}{\partial t} = \delta_\varepsilon(\phi) \left(\mu \mathrm{div} \left(\frac{\nabla \phi}{|\nabla \phi|} \right) - \lambda_1 (u_0 - c_1)^2 + \lambda_2 (u_0 - c_2)^2 \right) \tag{2.3}$$

where $\delta_\varepsilon(\phi)$ is an approximation of the Dirac function $\delta(\phi)$ and c_1, c_2 are updated by the formula

$$c_1 = \frac{\int_\Omega u_0 H(\phi) dx}{\int_\Omega H(\phi) dx}, \quad c_2 = \frac{\int_\Omega u_0 (1 - H(\phi))\, dx}{\int_\Omega (1 - H(\phi))\, dx}. \tag{2.4}$$

Chan-Vese model is extended to multiphase case in [6] which can deal with 2^n-phase segmentation using n level set functions. The corresponding formula is quite complicated and we omitted here.

2.3. Region Competition. Zhu and Yuille [22] proposed to minimize the following energy

$$F(\Gamma, \{\alpha_i\}) = \sum_{i=1}^{N} \left\{ \frac{\mu}{2} \int_{\partial \Omega_i} ds - \int_{\Omega_i} \log P_i (I|\alpha_i) dx \right\}. \tag{2.5}$$

The first term within the braces is the length of the boundary curve $\partial \Omega_i$ for region Ω_i. $\Gamma = \bigcup_{i=1}^{N} \partial \Omega_i$ is the segmentation boundaries of the entire image. The second term is the sum of the cost for coding the intensity I into region Ω_i by the conditional probability distributions $-\log P_i (I|\alpha_i)$ where α_i is the parameter in the probability density function P_i.

In order to solve a general two-phase region competition problem as minimizing

$$F(\Gamma, \alpha_1, \alpha_2) = \int_{\partial \Omega_1} ds + \lambda \int_{\Omega_1} r_1^{\alpha_1} dx + \lambda \int_{\Omega_2} r_2^{\alpha_2} dx,$$

where the image region Ω is partitioned into Ω_1 and Ω_2, α_i is the region parameter of the region R_i, and $r_i^{\alpha_i}$ is error function. Mory et al [17] proposed to use fuzzy membership function $u \in BV_{[0,1]}(\Omega)$ to represent the region and minimize the two-phase fuzzy region competition energy instead

$$F(u, \alpha_1, \alpha_2) = \int_\Omega |\nabla u| dx + \lambda \int_\Omega u r_1^{\alpha_1} dx + \lambda \int_\Omega (1 - u) r_2^{\alpha_2} dx. \tag{2.6}$$

The fast dual projection method proposed by Chambolle [8] is used to solve the problem.

3. The Proposed Method. We first write the general N-phase region competition functional as

$$F(\mathcal{R},\alpha)=\sum_{i=1}^{N}\left\{\int_{\partial\Omega_i}ds+\lambda\int_{\Omega_i}r_i^{\alpha_i}dx\right\} \tag{3.1}$$

where $\mathcal{R}=(\Omega_1,...,\Omega_N)$, $\alpha=(\alpha_1,...,\alpha_N)$ and $r_i^{\alpha_i}$ are error functions in region Ω_i. Three typical error functions exist in literatures are:

1. Chan-Vese model: $r_i^{\alpha_i}=(I-c_i)^2$, $\alpha_i=c_i$ are constants;
2. Region competition model: $r_i^{\alpha_i}=-\log P_i\left(I|\alpha_i\right)$. For example, if we choose the Gaussian kernel

$$P_i\left(I|\alpha_i\right)=\frac{1}{\sqrt{2\pi}\sigma_i}\exp\left(-\frac{(I-\mu_i)^2}{2\sigma_i^2}\right),$$

   then $\alpha_i=(\mu_i,\sigma_i)$ are scalars;
3. Mumford-Shah model: $r_i^{\alpha_i}=(I-s_i)^2+\mu\left|\nabla s_i\right|^2$, where $\alpha_i=s_i$ are functions.

In terms of characteristic functions $\chi=(\chi_1,...,\chi_N)$, where χ_i denotes the characteristic function of region Ω_i, the energy (3.1) can be rewritten as

$$E(\chi,\alpha)=\sum_{i=1}^{N}\int_{\Omega}|\nabla\chi_i|dx+\lambda\sum_{i=1}^{N}\int_{\Omega}r_i^{\alpha_i}\chi_i dx. \tag{3.2}$$

The term $\int_\Omega|\nabla\chi_i|dx$ equals the perimeter of Ω_i. There is a scaling of factor 2 since we add each boundary twice. For simplicity, we neglect it.

Binary value functions $\{\chi_i\}$ give a hard segmentation of Ω. In the following, we use a fuzzy membership function $u_i(x)$ to substitute the hard membership function χ_i in (3.2). Then we get our fuzzy region competition segmentation model of minimizing the energy functional

$$E(U,\alpha)=\sum_{i=1}^{N}\int_{\Omega}|\nabla u_i|dx+\lambda\sum_{i=1}^{N}\int_{\Omega}r_i^{\alpha_i}u_i^p dx \tag{3.3}$$

subject to

$$\text{(i)}\quad\sum_{i=1}^{N}u_i=1,\quad\text{(ii)}\quad 0\le u_i\le 1,\ \text{for } i=1:N,$$

where λ,p are positive parameters and p is to determine the fuzziness of segmentation.

3.1. Mathematical analysis. Here we choose Chan-Vese error function $r_i^{\alpha_i}=(I-c_i)^2$. Under the assumption the image $I\in L^2(\Omega)$, the energy (3.3) is well defined and finite for the admissible set

$$\text{adm}_N=\{U,c|u_i\in BV(\Omega),i=1:N,\text{satisfies (i) and (ii)},c\in\mathbb{R}^N\}.$$

We prove in the following the existence and symmetry of minimizer of energy E.

THEOREM 3.1. *(existence) Assume the image $I\in L^2(\Omega), I\ge 0$. Then for fixed parameters N,λ, there exists a minimizer of the energy E in admissible set adm_N.*

Proof. It is easy to derive from the Euler-Lagrange equation of energy E that

$$c_i = \frac{\int_\Omega I(x)u_i^p(x)dx}{\int_\Omega u_i^p(x)dx}$$

if $\int_\Omega u_i^p(x)dx > 0$. Otherwise, if $\int_\Omega u_i^p(x)dx > 0 (i.e.\ \ u_i(x) = 0\ a.e.\ x \in \Omega)$, we define $c_i = 0$.

If $I = 0\ a.e.\ x \in \Omega$, then $c_i = 0, i = 1 : N$. Hence $c_i = 0, i = 1 : N;\ u_1 = 1,\ u_j = 0, j = 2 : N$ is a minimizer. Otherwise, we take $u_1 = 1,\ u_j = 0,\ j = 2 : N;\ c_1 = \int_\Omega I dx/|\Omega|,\ c_j = 0,\ j = 2 : N$, then $E(U, c) = \int_\Omega (I - c_1)^2 dx < \infty$. Then the infimum of the energy must be finite. Let $(U^n, c^n) \subseteq \mathrm{adm}_N$ be a minimizing sequence for energy (3.3), that is, $E(U^n, c^n) \to \inf E(U, c)$. Then there exists a constant $M > 0$, such that

$$E(U^n, c^n) = \sum_{i=1}^N \int_\Omega |\nabla u_i^n| dx + \lambda \sum_{i=1}^N \int_\Omega (I - c_i^n)^2 (u_i^n)^p dx \le M.$$

Then we have each term of $E(U^n, c^n)$ is bounded, i.e.

$$\lambda \int_\Omega (I - c_i^n)^2 (u_i^n)^p dx \le M \tag{3.4}$$

$$\int_\Omega |\nabla u_i^n| dx \le M \tag{3.5}$$

Since u_i^n satisfies condition (i), $\|u_i^n\|_{L^1(\Omega)} = \int_\Omega u_i^n dx \le |\Omega|$. Together with (3.5) we get $\{u_i^n\}$ is uniformly bounded in $BV(\Omega)$ for each $i = 1 : N$. By the compactness property of BV space, up to a subsequence also denoted by $\{u_i^n\}$ after relabelling, there exists a function $u_i^* \in BV(\Omega)$ such that

$$\begin{aligned} &u_i^n \to u_i^* \ \text{ strongly in } L^1(\Omega) \\ &u_i^n \to u_i^* \ \text{ a.e. } x \in \Omega \\ &\nabla u_i^n \rightharpoonup \nabla u_i^* \ \text{ in the sense of measure.} \end{aligned}$$

Then by the lower semicontinuity of total variation,

$$\int_\Omega |\nabla u_i^*| dx \le \liminf_{n\to\infty} \int_\Omega |\nabla u_i^n| dx. \tag{3.6}$$

Meanwhile since u_i^n satisfies constraints (i)(ii), by convergence result, u_i^* also satisfies (i)(ii).

If c_i^n is given by

$$c_i^n = \frac{\int_\Omega I(u_i^n)^p dx}{\int_\Omega (u_i^n)^p dx}.$$

Set $w_i^n = \frac{(u_i^n)^p}{\int_\Omega (u_i^n)^p dx}$, then $0 \le w_i^n \le 1$. Otherwise, $c_i^n = 0$. Hence we get

$$0 \le c_i^n = \int_\Omega I w_i dx \le \int_\Omega I dx.$$

By the boundedness of sequence $\{c_i^n\}$, we can abstract a subsequence also denoted by $\{c_i^n\}$ and a constant c_i^* such that

$$c_i^n \to c_i^* \quad \text{uniformly.}$$

Finally, since $u_i^n \to u_i^*$, a.e. $x \in \Omega$ and $c_i^n \to c_i^*$, Fatou Lemma gives

$$\int_\Omega (I - c_i^*)^2 (u_i^*)^p dx \leq \liminf_{n\to\infty} \int_\Omega (I - c_i^n)^2 (u_i^n)^p dx \tag{3.7}$$

Combining inequalities (3.6) and (3.7) for all i, on a suitable subsequence, we have established that

$$E(U^*, c^*) \leq \liminf_{n\to\infty} E(U^n, c^n) = \inf E(U, c) \tag{3.8}$$

and hence (U^*, c^*) must be a minimizer. This completes the proof. □

Remark: The existence of minimizer of energy in the region competition method holds for error functions which follow a Gaussian distribution. It can be shown using the similar arguments in Theorem 3.1.

Let S_N denote the permutation group of $\{1, ..., N\}$. Each permutation $\gamma \in S_N$ is defined as a one to one map $\gamma : \{1, ..., N\} \to \{1, ..., N\}$ such that $(\gamma(1), ..., \gamma(N))$ is a rearrangement of $\{1, ..., N\}$. Denote $U_\gamma = (u_{\gamma(1)}, ..., u_{\gamma(N)})$, $c_\gamma = (c_{\gamma(1)}, ..., c_{\gamma(N)})$.

THEOREM 3.2. *(symmetry) For any permutation $\gamma \in S_N$, $E(U_\gamma, c_\gamma) = E(U, c)$. In particular, suppose that*

$$(U^*, c^*) = argmin_{(U,c)\in adm_N} E(U, c)$$

is a minimizer. Then for any $\gamma \in S_N$, (U_γ^*, c_γ^*) is also a minimizer of E.

The proof is straightforward and hence omitted.

4. Alternative Minimization. For efficiency of minimizing energy (3.3), we choose to follow [3, 17, 11] and take use of Chambolle's fast dual projection algorithm [8]. For that end we add auxiliary variables $V = (v_1, ..., v_N)$ and approximate E in (3.3) by

$$E_r(U, V, \alpha) = \frac{\lambda}{p} \sum_{i=1}^N \int_\Omega r_i^{\alpha_i} u_i^p dx + \sum_{i=1}^N \int_\Omega |\nabla v_i| dx + \frac{1}{2\theta} \sum_{i=1}^N \int_\Omega (v_i - u_i)^2 dx \tag{4.1}$$

where θ is chosen small enough so that u_i and v_i are almost identical with respect to the L^2 norm. Note that we use a scaling of λ with a factor $\frac{1}{p}$ for simplicity. We use alternative minimization method to minimize energy E_r.

4.1. Solve region parameters α. Fix U and V, we need to minimize

$$E_1(\alpha) = \sum_{i=1}^N \int_\Omega r_i^{\alpha_i} u_i^p dx$$

with respect to α. The solution of region parameters depends on the error function $r_i^{\alpha_i}$. Here we consider the Chan-Vese error function and its local version.

Let $r_i^{\alpha_i} = (I - c_i)^2$, then $\alpha = c$. Taking the derivative of $E_1(\alpha)$ with respect to c_i and setting the result to zero, we obtain the closed form solution

$$c_i = \frac{\int_\Omega I(x) u_i^p(x) dx}{\int_\Omega u_i^p(x) dx}. \tag{4.2}$$

Chan-Vese model assumes that the image can be approximated by piecewise constant function. In practice, images that could be accurately approximated by piecewise constant functions are rarely encountered. In some applications, this hypothesis holds locally. To that end, we extend the model to local case following [14, 17]. To realize localization, we introduce a symmetric Gaussian kernel function $\omega : \Omega \to \mathbb{R}$ satisfies

$$\int_\Omega \omega(x)dx = 1, \quad \omega(-x) = \omega(x).$$

Then the local error function at $y \in \Omega$ is

$$r_i^{\alpha_i}(y) = \int_\Omega \left(I(x) - s_i(y)\right)^2 \omega(y-x)\,dx \tag{4.3}$$

where the region parameter $\alpha_i = s_i$ is a function. Taking the derivative of $E_1(\alpha)$ with respect to the parameter s_i, we obtain

$$\int_\Omega u_i(x)\left(I(x) - s_i(y)\right)\omega(y-x)\,dx = 0.$$

Then we derive

$$s_i(y) = \frac{\int_\Omega v_i(x)\, I(x)\omega(y-x)\,dx}{\int_\Omega v_i(x)\omega(y-x)\,dx}$$

which can be simplified by convolution operator as

$$s_i = \frac{\omega * (v_i I)}{\omega * v_i}. \tag{4.4}$$

4.2. Solve auxiliary variables V. Fixing U and α, we solve v_i by minimizing

$$\int_\Omega |\nabla v_i| dx + \frac{1}{2\theta}\int_\Omega (v_i - u_i)^2 dx.$$

This problem can be efficiently solved by fast dual projection algorithm. The solution is given by

$$v_i = u_i - \theta \mathrm{div}\, p_i^*, \quad i = 1:N \tag{4.5}$$

where the vector p_i^* can be solved by fixed point method: Initializing $p_i^0 = 0$ and iterating

$$p_i^{n+1} = \frac{p_i^n + \tau\nabla\left(\mathrm{div}\, p_i^n - u_i/\theta\right)}{1 + \tau\left|\nabla\left(\mathrm{div}\, p_i^n - u_i/\theta\right)\right|} \tag{4.6}$$

with $\tau \le 1/8$ to ensure convergence. See [8] for more details.

4.3. Solve membership function U. Fixing V and c, we consider the optimization problem

$$\min E_2(U) = \frac{\lambda}{p}\sum_{i=1}^N \int_\Omega r_i^{\alpha_i} u_i^p dx + \frac{1}{2\theta}\sum_{i=1}^N \int_\Omega (v_i - u_i)^2 dx \tag{4.7}$$

subject to

$$\begin{array}{ll} \text{(i)} & \sum_{i=1}^N u_i(x) - 1 = 0 \\ \text{(ii)} & 0 \le u_i(x) \le 1, \text{ for } i = 1:N \end{array}$$

We give three methods to solve this optimization problem in the following.

4.3.1. Method I. We set $p = 1$ and relax constraint (i) by Lagrange multiplier method and minimize

$$E_{2a}(U) = \lambda \sum_{i=1}^{N} \int_\Omega r_i^{\alpha_i} u_i dx + \frac{1}{2\theta} \sum_{i=1}^{N} \int_\Omega (v_i - u_i)^2 dx + \frac{\nu}{2} \int_\Omega \left(\sum_{i=1}^{N} u_i - 1 \right)^2 dx \tag{4.8}$$

subject to

$$0 \le u_i(x) \le 1, \text{ for } i = 1 : N.$$

where ν is a positive Lagrange multiplier. Since the objective function is strictly convex and the feasible region is convex, it is a set of convex programming (CP) problems. Then there exists a unique global minimizer $U^* = (u_1^*, ..., u_N^*)$ of energy (4.8) and the following well known Karush-Kuhn-Tucker (KKT) conditions are both necessary and sufficient: Suppose U^* is the global minimizer of (4.8), then

(a) $u_i^*(x) \ge 0,\ 1 - u_i^*(x) \ge 0$
(b) There exist Lagrange multipliers $\beta_i^*(x)$ and $\gamma_i^*(x)$ for each point $x \in \Omega$ such that
$\frac{\partial E_{2a}(U)}{\partial u_i^*(x)} = \lambda r_i^{\alpha_i}(x) + \frac{1}{\theta}(u_i^*(x) - v_i(x)) + \nu \left(\sum_{i=1}^{N} u_i^* - 1 \right) = \beta_i^*(x) - \gamma_i^*(x)$
(c) $\beta_i^*(x) u_i^*(x) = 0,\ \gamma_i^*(x)(1 - u_i^*(x)) = 0$
(d) $\beta_i^*(x) \ge 0,\ \gamma_i^*(x) \ge 0$

for $i = 1 : N$.

We are aim to construct a set of functions $\{u_i, \beta_i, \gamma_i\}$ which satisfies the KKT conditions. First we assume $\tilde{U} = (\tilde{u}_1, ..., \tilde{u}_N)$ satisfies

$$\lambda r_i^{\alpha_i}(x) + \frac{1}{\theta}(\tilde{u}_i(x) - v_i(x)) + \nu \left(\sum_{i=1}^{N} \tilde{u}_i - 1 \right) = 0.$$

It is easy to check that the solution is

$$\tilde{u}_i = v_i - \lambda\theta r_i^{\alpha_i} - \frac{\nu\theta \left(\sum_{j=1}^{N} (v_j - \lambda\theta r_j^{\alpha_j}) - 1 \right)}{1 + N\nu\theta}.$$

Then we construct $\hat{u}_i$ by projecting $\tilde{u}_i$ on [0,1], that is

$$\hat{u}_i := \min\{\max\{\tilde{u}_i, 0\}, 1\}. \tag{4.9}$$

Let $\eta_i(x) = \lambda r_i^{\alpha_i}(x) + \frac{1}{\theta}(\hat{u}_i(x) - v_i(x)) + \nu \left(\sum_{j=1}^{N} \hat{u}_j - 1 \right)$. For each $x \in \Omega$, we choose $\hat{\beta}_i(x)$ and $\hat{\gamma}_i(x)$ as follows:

if $\hat{u}_i(x) \in (0, 1)$, then $\hat{\beta}_i(x) := 0$ and $\hat{\gamma}_i(x) := 0$;
if $\hat{u}_i(x) = 0$, then $\hat{\beta}_i(x) := \eta_i(x) \ge 0$ and $\hat{\beta}_i(x) := 0$;
if $\hat{u}_i(x) = 1$, then $\hat{\beta}_i(x) := 0$ and $\hat{\gamma}_i(x) := -\eta_i(x) \ge 0$.

It is easy to verify that $(\hat{u}_i, \hat{\beta}_i, \hat{\gamma}_i)$ satisfies KKT conditions (a)-(d). Therefore $\hat{U} = (\hat{u}_1, ..., \hat{u}_n)$ is a minimizer of energy(4.8). By the uniqueness of minimizer, we conclude $U^* = \hat{U}$.

4.3.2. Method II. We set $p = 1$ and relax constraint (i) by letting

$$u_N = 1 - \sum_{i=1}^{N-1} u_i.$$

Then we need to minimize

$$E_{2b}(\bar{U}) = \lambda \sum_{i=1}^{N-1} \int_\Omega (r_i^{\alpha_i} - r_N^{\alpha_N})\, u_i dx + \frac{1}{2\theta} \sum_{i=1}^{N-1} \int_\Omega (v_i - u_i)^2 dx dx \tag{4.10}$$

subject to

$$0 \le u_i(x) \le 1, \text{ for } i = 1 : N-1.$$

where $\bar{U} = (u_1, ..., u_{N-1})$. The objective function is strictly convex and the feasible region is convex, there exists a unique global minimizer $\bar{U}^* = (u_1^*, ..., u_{N-1}^*)$ of (4.10) and the following KKT conditions are both necessary and sufficient: Suppose $\tilde{U}^*$ is the global minimizer of (4.10), then

(a) $u_i^*(x) \ge 0,\ 1 - u_i^*(x) \ge 0$
(b) There exist Lagrange multipliers $\beta_i^*(x)$ and $\gamma_i^*(x)$ for each point $x \in \Omega$ such that
$\frac{\partial E_{2a}(U)}{\partial u_i^*(x)} = \lambda(r_i^{\alpha_i}(x) - r_N^{\alpha_N}(x)) + \frac{1}{\theta}(u_i^*(x) - v_i(x)) = \beta_i^*(x) - \gamma_i^*(x)$
(c) $\beta_i^*(x) u_i^*(x) = 0,\ \gamma_i^*(x)(1 - u_i^*(x)) = 0$
(d) $\beta_i^*(x) \ge 0,\ \gamma_i^*(x) \ge 0$

for $i = 1 : N-1$.

First we assume $\tilde{U} = (\tilde{u}_1, ..., \tilde{u}_{N-1})$ satisfies

$$\lambda(r_i^{\alpha_i}(x) - r_N^{\alpha_N}(x)) + \frac{1}{\theta}(\tilde{u}_i(x) - v_i(x)) = 0.$$

The solution is

$$\tilde{u}_i = v_i - \lambda\theta(r_i^{\alpha_i} - r_N^{\alpha_N}).$$

Then we construct $\hat{u}_i$ by projecting $\tilde{u}_i$ on [0,1], that is

$$\hat{u}_i := \min\{\max\{\tilde{u}_i, 0\}, 1\}. \tag{4.11}$$

Let $\eta_i(x) = \lambda\,(r_i^{\alpha_i}(x) - r_N^{\alpha_N}(x)) + \frac{1}{\theta}\,(\hat{u}_i(x) - v_i(x))$. For each $x \in \Omega$, we choose $\hat{\beta}_i(x)$ and $\hat{\gamma}_i(x)$ as follows:

if $\hat{u}_i(x) \in (0, 1)$, then $\hat{\beta}_i(x) := 0$ and $\hat{\gamma}_i(x) := 0$;
if $\hat{u}_i(x) = 0$, then $\hat{\beta}_i(x) := \eta_i(x) \ge 0$ and $\hat{\gamma}_i(x) := 0$;
if $\hat{u}_i(x) = 1$, then $\hat{\beta}_i(x) := 0$ and $\hat{\gamma}_i(x) := -\eta_i(x) \ge 0$.

It is easy to verify that $\{\hat{u}_i, \hat{\beta}_i, \hat{\gamma}_i\}$ satisfies KKT conditions (a)-(d). Therefore $\hat{U}$ is a minimizer of energy (4.10) and by uniqueness $\bar{U}^* = \hat{U}$.

4.3.3. Method III. Assume $p = 2$. We consider the optimization problem

$$\min E_{2c}(U) = \frac{\lambda}{2}\sum_{i=1}^{N}\int_{\Omega} r_i^{\alpha_i} u_i^2 dx + \frac{1}{2\theta}\sum_{i=1}^{N}\int_{\Omega}(v_i - u_i)^2 dx \tag{4.12}$$

subject to

$$\begin{array}{ll} \text{(i)} & \sum_{i=1}^{N} u_i(x) - 1 = 0 \\ \text{(ii)} & u_i(x) \geq 0, \text{ for } i = 1:N \\ \text{(iii)} & 1 - u_i(x) \geq 0, \text{ for } i = 1:N. \end{array}$$

Since the objective function is strictly convex and the feasible region is convex, there exists a unique global minimizer U^* of problem (4.12) and the following KKT conditions are both necessary and sufficient: Suppose U^* is the global minimizer of (4.12), then

(a) $\sum_{i=1}^{N} u_i^*(x) = 1$
(b) $u_i^*(x) \geq 0$ for $i = 1:N$
(c) There exist Lagrange multipliers $\delta^*(x), \beta_i^*(x), \gamma_i^*(x)$ for each point $x \in \Omega$ such that

$$\frac{\partial E_r(U)}{\partial u_i^*(x)} = \lambda r_i^{\alpha_i}(x) u_i^*(x) + \frac{1}{\theta}(u_i^*(x) - v_i(x)) = \delta^*(x) + \beta_i^*(x) - \gamma_i^*(x) \text{ for } i = 1:N$$

(d) $\beta_i^*(x) u_i^*(x) = 0,\ \gamma_i^*(x)(1 - u_i^*(x)) = 0$ for $i = 1:N$
(e) $\beta_i^*(x) \geq 0,\ \gamma_i^*(x) \geq 0$ for $i = 1:N$.

In order to construct a set of functions $(U, \delta, \beta_i, \gamma_i)$ which satisfies the KKT conditions, first we assume $\tilde{U}$ satisfies

$$\lambda r_i^{\alpha_i}(x)\tilde{u}_i(x) + \frac{1}{\theta}(\tilde{u}_i(x) - v_i(x)) = \delta(x).$$

Then the closed form solution of $\tilde{u}_i$ is given by

$$\tilde{u}_i = \frac{v_i - \theta\delta}{1 + \lambda\theta r_i^{\alpha_i}}.$$

Using the condition $\sum_{i=1}^{N} \tilde{u}_i = 1$, we have

$$\sum_{i=1}^{N} \frac{v_i - \theta\delta}{1 + \lambda\theta r_i^{\alpha_i}} = 1,$$

then

$$\delta = \frac{\sum_{i=1}^{N} \frac{v_i}{1+\lambda\theta r_i^{\alpha_i}} - 1}{\theta \sum_{i=1}^{N} \frac{1}{1+\lambda\theta r_i^{\alpha_i}}}. \tag{4.13}$$

Substituting δ into the formula of $\tilde{u}_i$ gives

$$\tilde{u}_i = \frac{v_i}{1 + \lambda\theta r_i^{\alpha_i}} - \frac{\sum_{j=1}^{N} \frac{v_j}{1+\lambda\theta r_j^{\alpha_j}} - 1}{\sum_{j=1}^{N} \frac{1+\lambda\theta r_i^{\alpha_i}}{1+\lambda\theta r_j^{\alpha_j}}}.$$

Then we can use $\tilde{u}_i$ in our construction. Project $\tilde{u}_i$ on [0,1] yields

$$\tilde{u}_{i_{proj}} = \min\{\max\{\tilde{u}_i, 0\}, 1\}.$$

Since it is easy to check that $\sum_{i=1}^{N} \tilde{u}_i = 1$, then $\sum_{j=1}^{N} \tilde{u}_{j_{proj}}$ must be positive. Now we can define

$$\hat{u}_i(x) := \frac{\tilde{u}_{i_{proj}}}{\sum_{j=1}^{N} \tilde{u}_{j_{proj}}}. \tag{4.14}$$

Let $\eta_i(x) = \lambda r_i^{\alpha_i}(x) + \frac{1}{\theta}(\hat{u}_i(x) - v_i(x))$. For each $x \in \Omega$, we choose $\hat{\delta}(x)$, $\hat{\beta}_i(x)$ and $\hat{\gamma}_i(x)$ as follows:

if $\hat{u}_i(x) \in (0,1)$, then

$$\begin{aligned} &\hat{\delta}(x) := \delta, \\ &\hat{\beta}_i(x) := 0, \\ &\hat{\gamma}_i(x) := 0; \end{aligned}$$

if $\hat{u}_i(x) = 0$, then

$$\begin{aligned} &\hat{\delta}(x) := -\max_{1\le j\le N} |\eta_j(x)|, \\ &\hat{\beta}_i(x) := \eta_i(x) + \max_{1\le j\le N} |\eta_j(x)| \ge 0, \\ &\hat{\gamma}_i(x) := 0; \end{aligned}$$

if $\hat{u}_i(x) = 1$, then

$$\begin{aligned} &\hat{\delta}(x) := -\max_{1\le j\le N} |\eta_j(x)|, \\ &\hat{\beta}_i(x) := 0, \\ &\hat{\gamma}_i(x) := \eta_i(x) + \max_{1\le j\le N} |\eta_j(x)| \ge 0. \end{aligned}$$

It is easy to verify that $\{\hat{u}_i, \hat{\delta}, \hat{\beta}_i, \hat{\gamma}_i\}$ satisfies KKT conditions (a)-(e). Therefore $\hat{U}$ is a minimizer of problem (4.12) and by uniqueness $U^* = \hat{U}$.

Remark: Besides the above setting, we can set $p = 2$ in Methods I and II, and set $p = 1$ in Method III, their corresponding solutions can be obtained by using the similar techniques, thus is omitted. For $p \neq 1, 2$, the closed form solution cannot be obtained. Numerical optimization computation must be used. On the other hand, in the special case of $N = 2$, our Method II is similar to the algorithm in [17], see (2.6). Methods I and III are new and novel even for two-phase image segmentation.

4.4. Algorithm details. We choose Chan-Vese error function as an example to describe the algorithm of minimizing E_r. The algorithm can be summarized in the following steps:

- Initialization: Initialize the membership functions u_i^0 such that the constraint (i) and (ii) are both satisfied. $v_i^0 = u_i^0, c_i^0 = 0$.
- Iteration: Update c_i^k by formula (4.2);
  Update v_i^k by formula (4.5);
  Update u_i^k by formula (4.9) in Method I, (4.11) in Method II or (4.14) in Method III.

- Termination criterion:

$$\|c^k - c^{k-1}\| \leq \epsilon$$

where $c^k = (c_1^k, ..., c_N^k)$ is the vector of centers and $\|\cdot\|$ denotes the Euclidean distance and ϵ is a small positive number defined by the user.

We remark that in above iterations when we update v_i^k by formula (4.5), and get the p_i^* in (4.5), we only need to iterate (4.6) one time with initial value p_i^0 equals to the p_i^* value in the last loop of alternative minimization. It is well-known that the original Chambolle's dual projection algorithm set $p_i^0 = 0$. Our initialization makes use of the information of p_i^* obtained in the last loop in the alternative minimization process and is more efficient. In our algorithm, the solution of membership functions and region parameters are given by closed form solution, meanwhile the auxiliary variables can be solved by one iteration of Chambolle's projection, so that the algorithm is very efficient. In contrast, in the level set counterpart of our model, for example, the Chan-Vese model, the level set functions are solved by gradient descent method with a small time step and hence is slow.

4.5. Convergence of the algorithm. For simplicity, we choose the Chan-Vese error function. By running the algorithm, we get sequences:

$$(c_i^0, v_i^0, u_i^0, c_i^1, v_i^1, u_i^1, ..., c_i^k, v_i^k, u_i^k, ...).$$

We introduce the simplified notation (U^k, V^k, c^k) to denote all these sequences. We show here that our algorithm gives a coordinate minimum of the constrained problem (4.1).

THEOREM 4.1. *There exists a subsequence of (U^k, V^k, c^k) which converges to a coordinate minimum of E_r on $X = BV_{[0,1]}(\Omega)^N \times BV(\Omega)^N \times \mathbb{R}^N$.*

Proof. As we solve alterative minimization problems, we have

$$\begin{aligned} &E_r(U^{k+1}, V^{k+1}, c^{k+1}) \leq E_r(U^{k+1}, V^{k+1}, c^k) \\ &\leq E_r(U^{k+1}, V^k, c^k) \leq E_r(U^k, V^k, c^k). \end{aligned} \tag{4.15}$$

In particular, the sequence $E_r(U^k, V^k, c^k)$ is nonincreasing and bounded by zero. Thus it converges in $\mathbb{R}$. Denote the limit by m, that is

$$m = \lim_{k\to\infty} E_r(U^k, V^k, c^k).$$

Similar to that in the proof of Theorem 3.1, we can prove that E_r is coercive. As the sequence $E_r(U^k, V^k, c^k)$ converges, we deduce that the sequence (U^k, V^k, c^k) is bounded in X. Hence we can extract a subsequence $(U^{k_n}, V^{k_n}, c^{k_n})$ which converges to $(\hat{U}, \hat{V}, \hat{c}) \in X$ as $k_n \to \infty$. Moreover, for all $k_n \in \mathbb{N}$ and all $U \in BV_{[0,1]}(\Omega)^N$

$$E_r(U^{k_n+1}, V^{k_n}, c^{k_n}) \leq E_r(U, V^{k_n}, c^{k_n}), \tag{4.16}$$

for all $k_n \in \mathbb{N}$ and all $V \in BV(\Omega)^N$

$$E_r(U^{k_n}, V^{k_n+1}, c^{k_n}) \leq E_r(U^{k_n}, V, c^{k_n}), \tag{4.17}$$

and for all $k_n \in \mathbb{N}$ and $c \in \mathbb{R}^n$

$$E_r(U^{k_n}, V^{k_n}, c^{k_n+1}) \leq E_r(U^{k_n}, V^{k_n}.c), \tag{4.18}$$

Let us denote by $\tilde{V}$ a cluster of V^{k_n+1}. Since E_r is continuous on X, by (4.15), we have

$$m = E_r(\hat{U}, \hat{V}, \hat{c}) = E_r(\hat{U}, \tilde{V}, \hat{c}).$$

By formula (4.5), we have

$$v_i^{k_n+1} = u_i^{k_n} - \theta \mathrm{div}\, p_i^*(u_i^{k_n}), \tag{4.19}$$

where $p_i^*(u_i^{k_n})$ means p_i^* is dependent on $u_i^{k_n}$. By passing the limit in (4.19), we get

$$\tilde{v}_i = \hat{u}_i - \theta \mathrm{div}\, p_i^*(\hat{u}_i), \tag{4.20}$$

and then $\tilde{v}_i = \hat{v}_i$, i.e., $\tilde{V} = \hat{V}$. By (4.2), the closed form solution of $c_i^{k_n+1}$ is

$$c_i^{k_n+1} = \frac{\int_\Omega I(u_i^{k_n})^p dx}{\int_\Omega (u_i^{k_n})^p dx}.$$

By passing the limit we get $c^{k_n+1} \to \hat{c}$. Since $u_i^{k_n+1}$ is given by a closed form solution related with V^{k_n} and c^{k_n}, it is easy to conclude that $U^{k_n+1} \to \hat{U}$. By passing the limit in (4.16), (4.17) and (4.18), we have for all $U \in BV_{[0,1]}(\Omega)^N$

$$E_r(\hat{U}, \hat{V}, \hat{c}) \leq E_r(U, \hat{V}, \hat{c}), \tag{4.21}$$

for all $k_n \in \mathbb{N}$ and all $V \in BV(\Omega)^N$

$$E_r(\hat{U}, \hat{V}, \hat{c}) \leq E_r(\hat{U}, V, \hat{c}), \tag{4.22}$$

and for all $k_n \in \mathbb{N}$ and $c \in \mathbb{R}^n$

$$E_r(\hat{U}, \hat{V}, \hat{c}) \leq E_r(\hat{U}, \hat{V}, c). \tag{4.23}$$

(4.21), (4.22) and (4.23) can respectively be rewritten as

$$E_r(\hat{U}, \hat{V}, \hat{c}) = \inf_U E_r(U, \hat{V}, \hat{c}), \tag{4.24}$$

$$E_r(\hat{U}, \hat{V}, \hat{c}) = \inf_V E_r(\hat{U}, V, \hat{c}), \tag{4.25}$$

$$E_r(\hat{U}, \hat{V}, \hat{c}) = \inf_c E_r(\hat{U}, \hat{V}, c), \tag{4.26}$$

Then we have for $i = 1 : N$

$$0 \in \frac{\partial E_r}{\partial u_i}, 0 \in \frac{\partial E_r}{\partial u_i}, 0 \in \frac{\partial E_r}{\partial c_i}.$$

Finally we can conclude that $(\hat{U}, \hat{V}, \hat{c})$ is a coordinatewise minimum with energy $E_r(\hat{U}, \hat{V}, \hat{c}) = m$. □

5. Extension to Vector-valued Images. It is straightforward to extend the algorithm for vector-valued images. Assume $I : \Omega \to \mathbb{R}^m$ be the vector-valued image, then the Chan-Vese error of the j-th channel is defined by

$$r_{i,j}^{c_{i,j}} = (I_j - c_{i,j})^2.$$

The i-th error function is then the average of the errors of the m channels, that is

$$r_i^{c_i} = \frac{r_{i,1}^{c_{i,1}} + \cdots + r_{i,m}^{c_{i,m}}}{m}$$

where $c_i = (c_{i,1}, ..., c_{i,N})$ is a vector. It is easy to derive the formula of $c_{i,j}$, which is

$$c_{i,j} = \frac{\int_\Omega I_j(x) u_i^p(x) dx}{\int_\Omega u_i^p(x) dx}$$

if $\int_\Omega u_i^p(x)dx > 0$; otherwise $c_{i,j} = 0$. Then the numerical algorithm just follows the algorithm in in Section 4 for gray images by using new formulas for c_i and $r_i^{c_i}$ and thus is omitted.

6. Experimental Results. We test our algorithm on synthetic images, and real (gray scale and color) images. We test all the three Methods I, II, III to solve membership functions. In all the experiments, we choose Chan-Vese error function or its local version. Some parameters are fixed as follows: $\theta = 0.1, \nu = 1000, \epsilon = 10^{-4}$. The parameter λ is required to be tuned for each image. In the proposed algorithm, only the membership functions need to be initialized. The default of initial membership functions is random initialization, i.e., we initialize the membership functions u_i by random matrices where each entry follows an uniform distribution $[0, 1]$, and then we normalize them such that the membership constraints are satisfied. We also consider a special initialization in two-phase image segmentation. We draw a circle on the image and set the membership function $u_1^0 = 1$ inside the circle and $u_1^0 = 0$ outside, while set $u_2^0 = 1 - u_1^0$. The circle is in green color. In all the experiments, the final segmentation results are obtained by checking the class where its membership function value at the pixel is the largest among all membership functions.

6.1. Two-phase segmentation. Two-phase segmentation of gray scale images with Chan-Vese error function are reported in Figures 6.1-6.3. It is showed that our fuzzy model retains the advantages of the level set based Chan-Vese model. Indeed, we can segment objects whose boundaries cannot be defined or are badly defined through gradient. This includes, for example, smeared boundaries (see Figures 6.2(d) and 6.3(b)) and cognitive contours (boundaries of larger objects defined by grouping smaller ones, see Figure 6.1) [1].

We use Method I to solve membership functions as shown in Figure 6.1. In the procedure of tuning the parameter λ, we observe that the value of λ affects greatly the segmentation result. For $\lambda = 0.0002$, in Figure 6.1(a), the initial and the final segmentation are marked with green and red contours respectively, The result shows our algorithm can get cognitive contours. The corresponding two membership functions are displayed in Figures 6.1(b) and 6.1(c). Figures 6.1(d) and 6.1(g) give the segmentation results for $\lambda = 0.01$ and $\lambda = 10$ respectively. Their corresponding membership functions are also shown in Figures 6.1(e)-(f) and Figures 6.1(h)-(i) respectively. We note that random initialization is used to obtain the results in Figures 6.1(d) and 6.1(g). We also find that when λ is in the range of $[0.0005, 1]$, we get the

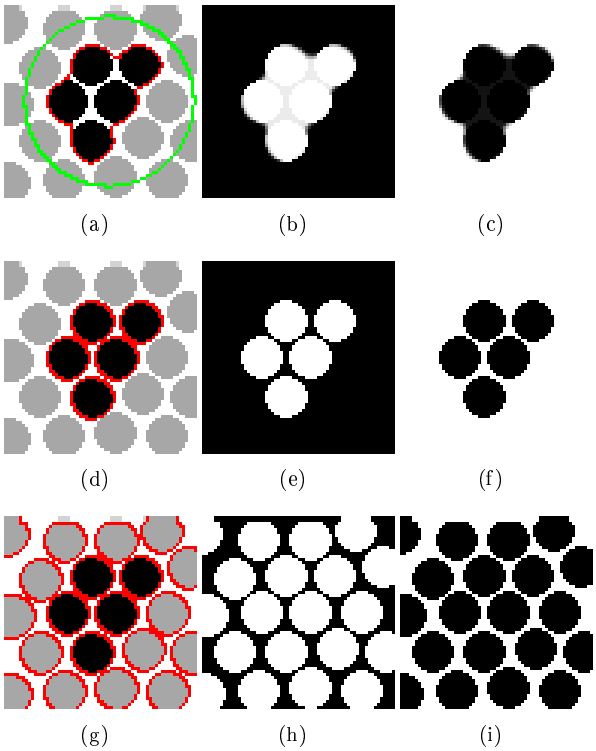

FIG. 6.1. *Two-phase segmentation. The test image is of size* 64×64. *(a) the contour of the initial guess (green) and the contour of the final segmentation (red) with* $\lambda = 0.0002$*; (b)-(c) the membership functions in (a); (d) the segmentation result with* $\lambda = 0.01$*; (e)-(f) the membership functions in (d); (g) the segmentation result with* $\lambda = 10$*; (h)-(i) the membership functions in (g).*

same segmentation result as shown in Figure 6.1(d). When $\lambda \geq 10$, we obtain the same segmentation result as shown in Figure 6.1(g).

Next we use Method I to perform image segmentation for the galaxy image as shown in Figure 6.2. In the figures, we show the intermediate and final segmentation results. We find that the algorithm can obtain the smeared contours of galaxy.

In Figure 6.3, we also use Method I to perform image segmentation for a case of smooth boundary detection. In this example, we consider random initialization of membership functions. When λ is set to 0.1, the segmentation result is shown in Figure 6.3(b), and the corresponding membership functions are shown in Figures 6.3(c)-(d). Indeed, for a quite large range of λ (0.001-1000), we obtain the same segmentation result as shown in Figure 6(b).

In the last three examples, when Methods II and III are used, similar segmentation results are obtained.

We remark that the proposed model has improved the hard partition algorithm by assigning membership function value to pixels in different regions. These membership function (fuzzy) values can be used to decide the core and boundary pixels in the regions, thereby providing more useful information for dealing with boundary pixels. For instance, some of the boundary pixels generated by the proposed method have membership function values are not close to 1 or close to 0.

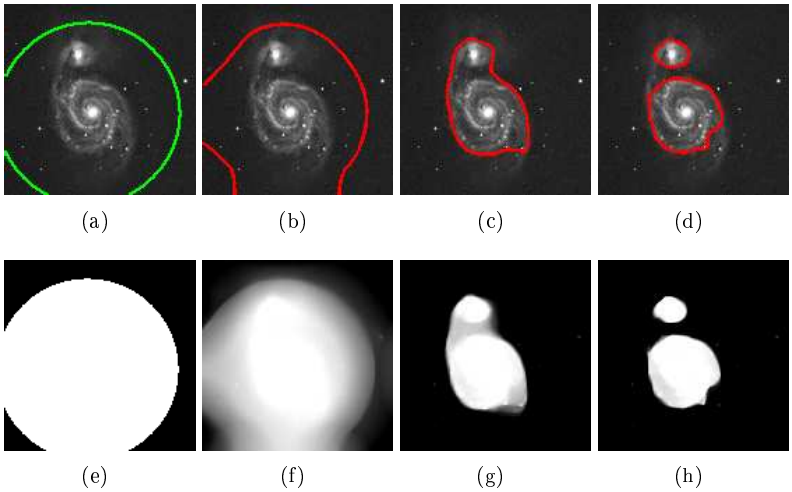

FIG. 6.2. *Two-phase segmentation. The test image is of size* 137×137 *and* $\lambda = 0.0001$ *is set. (a) the contour of the initial guess (green) (b)-(c) the intermediate segmentations (red); (d) the final segmentation (red); (e) the initial membership functions; (f)-(g) the intermediate membership functions; (h) the final membership.*

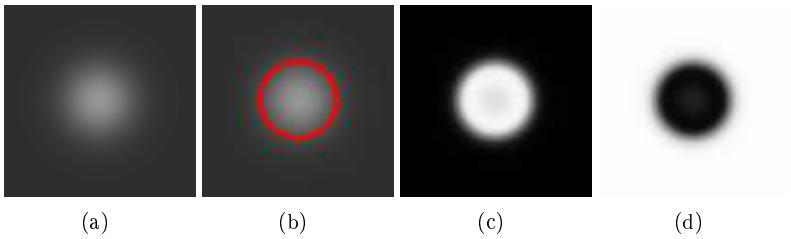

FIG. 6.3. *Two-phase segmentation. The test image is of size* 100×100 *and* $\lambda = 0.1$ *is set. (b) the segmentation result; (c)-(d) the membership functions.*

6.2. Multi-phase segmentation. In this subsection, we test the proposed methods for multi-phase image segmentation of gray scale and color images. In these examples, we use the Chan-Vese error function.

In the first example, we show the three-phase segmentation results using Method II. Figure 6.4(b) shows the piecewise constant approximation (three constants) of the test image given in Figure 6.4(a). The corresponding membership functions are displayed in Figures 6.4(c)-(e) respectively.

In the second example, we show the five-phase segmentation results using Method III. The test image is contaminated by zero mean Gaussian noise with standard deviation 10, see Figure 6.5(a). Figure 6.5(b) shows the piecewise constant approximation (five constants) of the test image. The corresponding membership functions are displayed in Figures 6.5(c)-(g) respectively.

In the third example, we show the three-phase color segmentation results using Method I. The test image in Figure 6.6(a) contains some textures in the background. Figure 6.6(b) shows the piecewise constant approximation (three color vectors) of the test image. The corresponding membership functions are displayed in Figures 6.6(c)-(e) respectively.

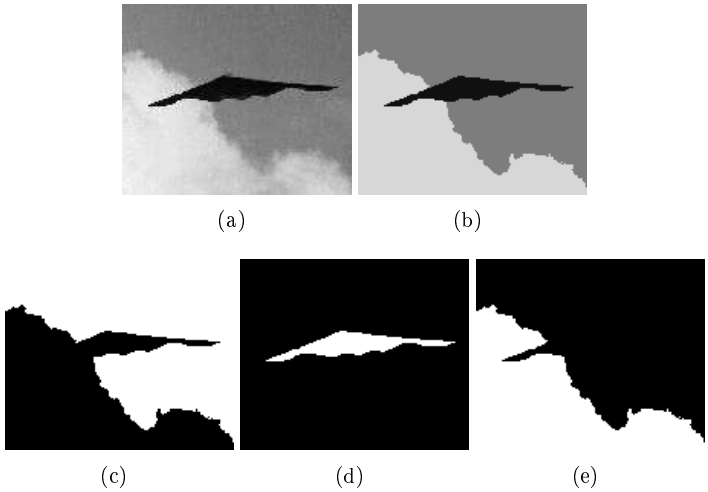

FIG. 6.4. *Three-phase segmentation using Method II with* $\lambda = 0.2$. *(a) the test image is of size* 150×125*; (b) the piecewise constant image; (c)-(e) membership functions* u_1, u_2, u_3.

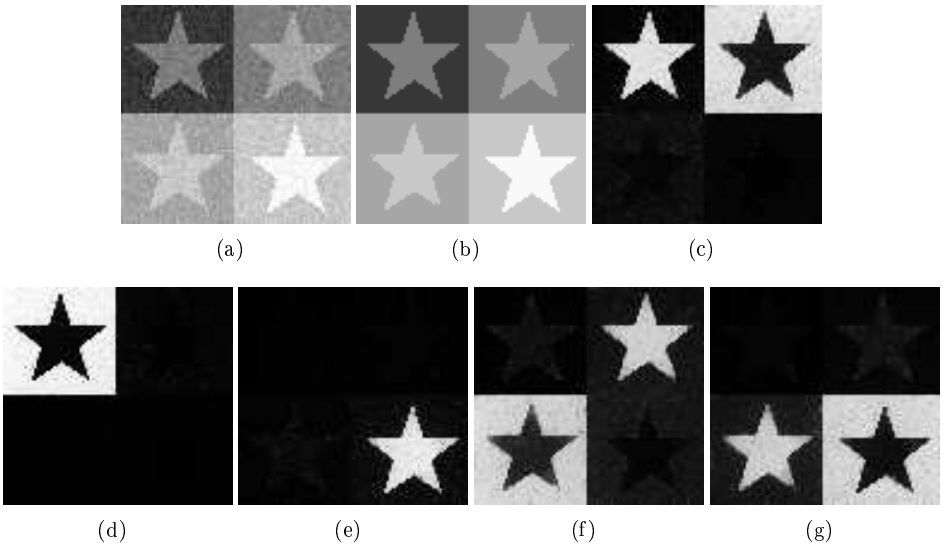

FIG. 6.5. *Five-phase segmentation using Method III with* $\lambda = 0.005$. *(a) the test image is of size* 96×91 *and Gaussian noise with zero mean and standard deviation 10 is added; (b) the piecewise constant image; (c)-(g) membership functions* u_1, u_2, u_3, u_4, u_5.

In the fourth example, we show the six-phase color segmentation results using Method III. The test image is a synthetic image and zero mean Gaussian noise with standard deviation 50 is added, see Figure 6.7(a). Figure 6.7(b) shows the piecewise constant approximation (six color vectors) of the test image. The corresponding membership functions are displayed in Figures 6.7(c)-(h) respectively.

In the figures, we only present the segmentation results by one of the proposed methods, Methods I, II and III indeed can provide similar segmentations results in the above examples.

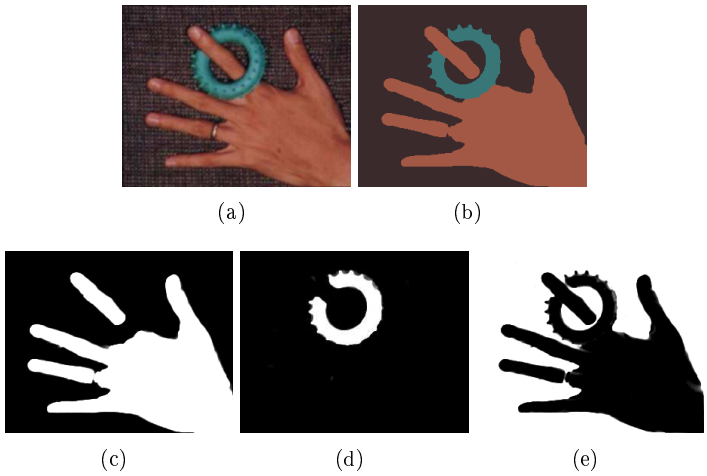

FIG. 6.6. *Three-phase color segmentation using Method I with* $\lambda = 0.01$. *(a) the test image is of size* 303×241*; (b) the piecewise constant color image; (c)-(e) the membership functions* u_1, u_2, u_3.

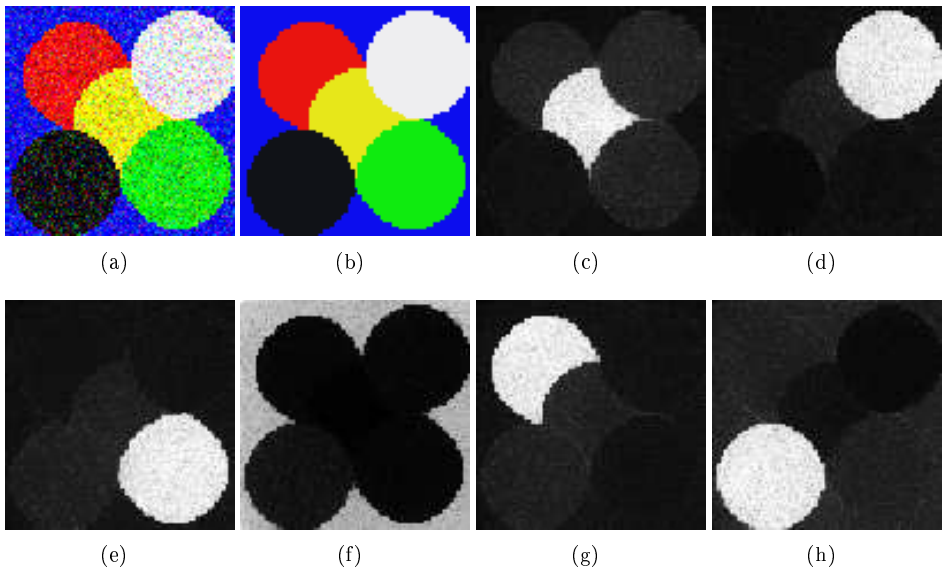

FIG. 6.7. *Six-phase color segmentation using Method III with* $\lambda = 0.0005$. *(a) the test image is of size* 100×100 *and is contaminated by Gaussian zero mean noise with standard deviation 50; (b) the piecewise constant color image; (c)-(h) the membership functions* $u_1, u_2, u_3, u_4, u_5, u_6$.

According to the above examples on gray scale and color images, they have demonstrated the effectiveness of the proposed methods.

6.3. Comparison with other segmentation methods. In this subsection, we compare the proposed method with other segmentation methods.

In the first example, we consider the comparison of two-phase segmentation with different methods. Figure 6.8(a) is a test vessel image with inhomogeneous intensity. With Chan-Vese error function and Method I, our algorithm fails to delineate out

the boundary of vessel, see Figure 6.8(c). The level set based Chan-Vese model also fails, see Figure 6.4(d). In contrast, with local error function (4.3) and Method I, our algorithm can give a more satisfactory result in Figure 6.8(b). Here we use the same initialization to obtain the segmentation results in Figures 6.8(b)-(d). We remark that with local error function, Methods II and III also works and the segmentation results are similar to that in Figure 6.8(b).

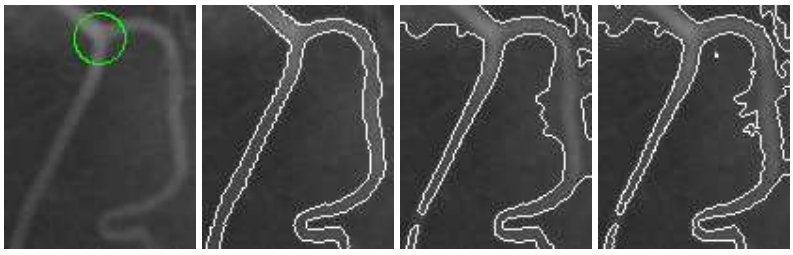

(a) (b) (c) (d)

FIG. 6.8. *Two-phase segmentation. (a) the test image is of size* 102×130 *with the initial guess (the green contour); (b) the segmentation result using Method I and local error function (4.3) with* $\lambda = 0.01$*; (c) the segmentation result using Method I and the Chan-Vese error function with* $\lambda = 0.01$*; (d) the segmentation result using the level set based Chan-Vese model.*

In the second example, we show the proposed algorithm with the method in [16] for four-phase image segmentation. Figure 6.9(a) is the noisy test image. Figures 6.9(b)-(f) show the piecewise constant approximation and the four membership functions using the proposed algorithm (Method III). We employ the method in [16] with the parameters: dt=0.0004, beta=1.5, r=2.5. The segmentation results are given in Figures 6.10, 6.11 and 6.12 for different initial piecewise constants. In order to quantify the segmentation results, we use segmentation accuracy which is defined as the ratio of the number of rightly classified pixels and the total number of pixels. The experiment results show that the segmentation accuracy and computational time of the method in [16] is quite sensitive to the initialization of piecewise constants. With a good initial piecewise constants, the method is very fast and the image can be segmented correctly. However, when the initial piecewise constants are far away from the suitable values, the computational time increases and the segmentation accuracy decreases. In contrast, our algorithm can give an accurate segmentation using random membership functions in Figure 6.9. These results show our algorithm is less sensitive to initialization.

In the third example, we compare our algorithm (Method III) with the level set method based Chan-Vese model for four-phase segmentation. The piecewise constant segmentation result of our algorithm is showed in Figure 6.13(b) and the membership functions are showed in Figures 6.13(c)-(f). For the four-phase Chan-Vese model, two level sets ϕ_1, ϕ_2 are needed. Figure 6.13(g) and Figure 6.13(h) display the initial and the final zero level sets. Figure 6.13(i) shows the piecewise constant image given by formula $\sum_{i=1}^{4} c_i \chi_{\Omega_i}$ where $\chi_{\Omega_i}, i = 1:4$ are the characteristics functions of the following four regions: $\Omega_1 = \{x | \phi_1(x) \geq 0, \phi_2(x) \geq 0\}$, $\Omega_2 = \{x | \phi_1(x) \geq 0, \phi_2(x) < 0\}$, $\Omega_3 = \{x | \phi_1(x) < 0, \phi_2(x) \geq 0\}$, $\Omega_4 = \{x | \phi_1(x) < 0, \phi_2(x) < 0\}$. It is obvious that our segmentation result in Figure 6.13(b) is more accurate than the result in Figure 6.13(i). We also compare the computational times of the two methods. Our algorithm converges at 52 iterations consuming 7.1 seconds, while the Chan-Vese model

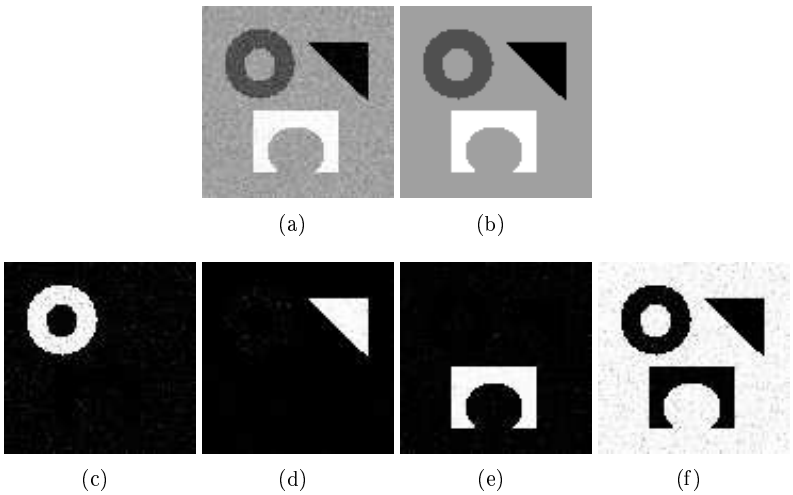

FIG. 6.9. *Four-phase segmentation. (a) the test is of size* 90×90 *and it is contaminated by Gaussian noise with zero mean and standard deviation 10; (b) the piecewise constant image by Method III with* $\lambda = 0.05$*; (c)-(f) the membership functions* u_1, u_2, u_3, u_4*; [computational time = 0.9 seconds, number of iteration = 42, segmentation accuracy = 100%].*

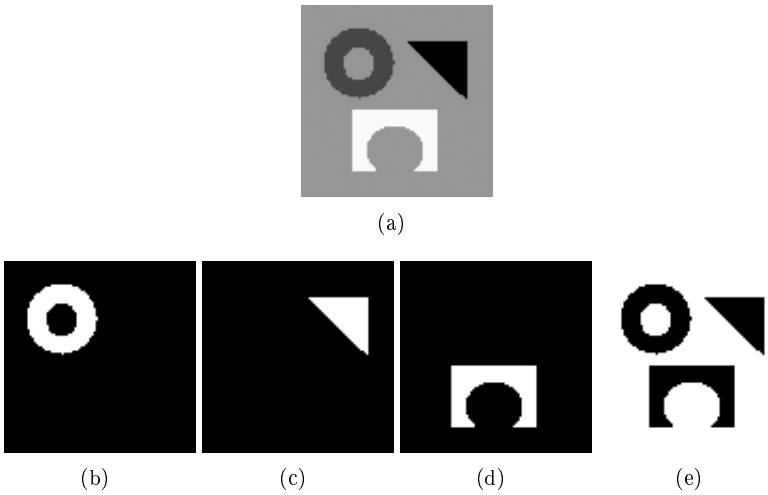

FIG. 6.10. *(a) the piecewise constant image by the method in [16] with initial piecewise constants* $c = [0, 70, 150, 250]$*; (b)-(e) the four phases; [computational time = 1 second, segmentation accuracy = 100%].*

converges at 100 iterations consuming 14.5 seconds. Remark that in our implementation of Chan-Vese model, in order to make the Chan-Vese algorithm more efficient, we use $|\nabla \phi_i|$ instead of $\delta_\epsilon(\phi_i)$ in the evolution equation where ϕ_i are the level set functions.

7. Concluding Remarks. In this paper we have developed the fuzzy region competition framework. The framework is general due to the freedom of choice of error functions. With different error function, only the minimization of region parameters

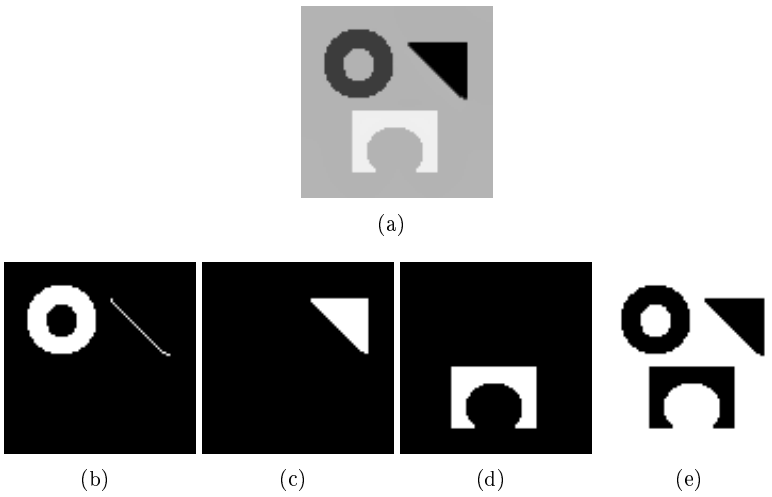

(a)

(b) (c) (d) (e)

FIG. 6.11. *(a) the piecewise constant image by the method in [16] with initial piecewise constants* $c = [0, 60, 180, 240]$*; (b)-(e) the four phases; [computational time = 63 seconds, segmentation accuracy = 99.67%].*

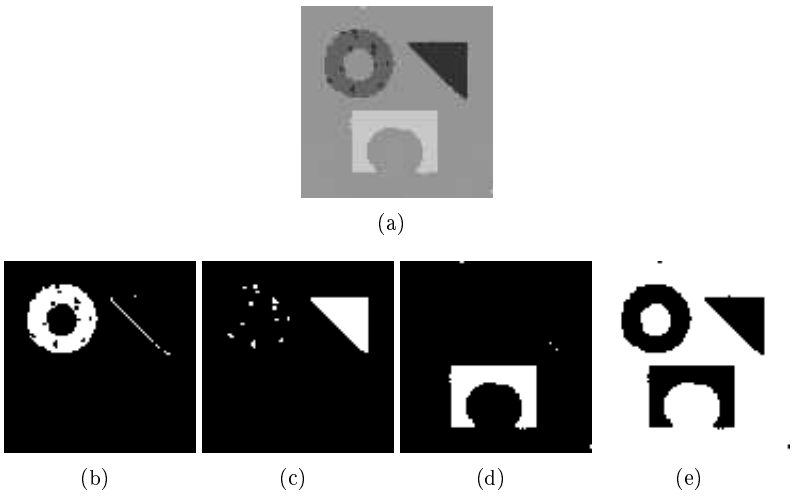

(a)

(b) (c) (d) (e)

FIG. 6.12. *(a) the piecewise constant image by the method in [16] with initial piecewise constants* $c = [50, 100, 150, 200]$*; (b)-(e) the four phases; [computational time = 73 seconds, segmentation accuracy = 98.94%].*

is different, while the minimization of membership functions and auxiliary variables remains unchanged. In the future work, we will consider the Mumford-Shah error function and nonparametric error function. It is expected that the latter models can deal with complex images such as low resolution medical images and texture images.

Acknowledgement. The authors would like to thank Prof. X.-C. Tai and E. Bae for the source code of [16]. The authors would also like to thank the two referees for their useful suggestions to the manuscript.

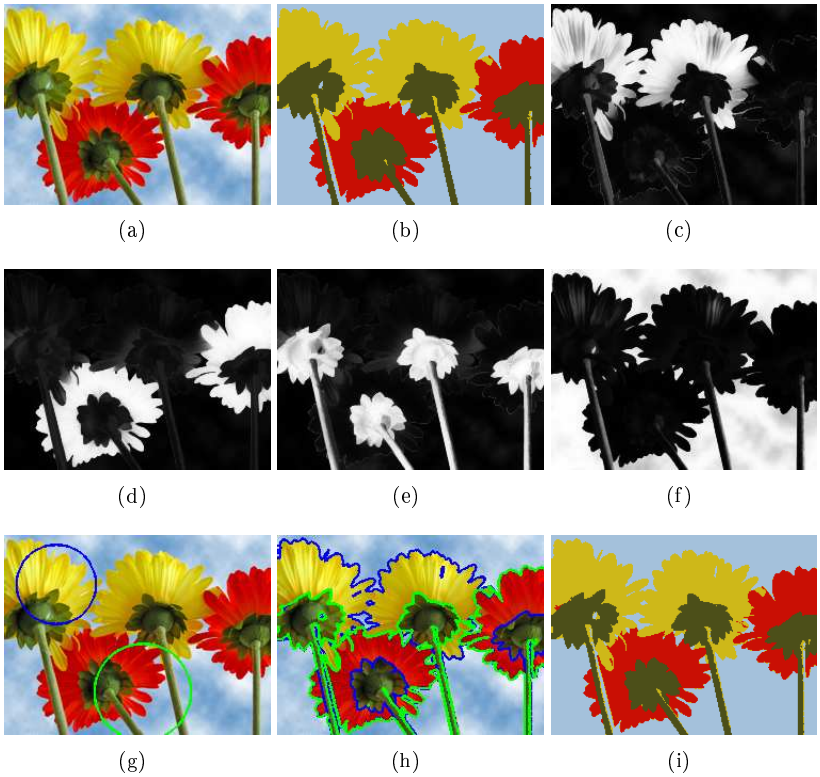

FIG. 6.13. *Four-phase color image segmentation. (a) the test image is of size* 250×188*; (b) the piecewise constant image by Method III with* $\lambda = 0.002$*; piecewise constant image; (c)-(f) the membership functions* u_1, u_2, u_3, u_4*; [computational time = 7.1 seconds and number of iterations = 52]; (g) the initial zero level sets; (h) the final zero level sets; (i) the piecewise constant image by the Chan-Vese model [computational time = 14.5 seconds and number of iterations = 100].*

REFERENCES

[1] G. Aubert and P. Kornprobst, Mathematical Problems in Image Processing: Partial Differential Equations and the Calculus of Variations (Applied Mathematical Sciences), Springer-Verlag, 2006, 2 Edition.

[2] J. C. Bezdek, L. O. Hall, and L. P. Clarke, Review of MR image segmentation techniques using pattern recognition, Med. Phys., 20(1993), pp. 1033-1048.

[3] X. Bresson, S. Esedoglu, P. Vandergheynst, J.-P. Thiran, S. Osher, Fast Global Minimization of the Active Contour/Snake Model, J. Math. Imaging Vis., 28(2007), pp. 151-167, 2007.

[4] V. Caselles, R. Kimmel, and G. Sapiro, Geodesic active contours, International Journal of Computer Vision, 1(1997), pp. 61-79.

[5] T. F. Chan and L. A. Vese, Active contour without edges, IEEE Trans. Image Process., 10(2001), pp. 266-277.

[6] T. F. Chan, B. Sandberg, and L. Vese. Active contours without edges for vector-valued images. J. Visual Communication Image Representation. 11(2000), pp. 130-141.

[7] T. F. Chan, S. Esedoglu, and M. Nikolova, Algorithms for finding global minimizers of image segmentation and denoising models, SIAM J. Appl. Math. 66(2006), pp. 1632-1648.

[8] A. Chambolle, An algorithm for total variation minimization and applications, J. Math. Imaging Vis., 20(2004), pp. 89-97.

[9] G. Chung and L.A. Vese, Image segmentation using a multilayer level-set approach, Comput. Visual. Sci. online, 2008.

[10] N. Houhou, J.P.Thiran and X. Bresson, Fast texture segmentation model based on the shape operator and active contour, IEEE Conference on Computer Vision and Pattern Recogni-

tion, CVPR 2008.
[11] Y. Huang, M. Ng and Y. Wen, A Fast Total Variation Minimization Method for Image Restoration, SIAM Journal on Multiscale Modeling and Simulation, 7(2008), pp. 774–795.
[12] Y. Jung, S. Kang and J. Shen, Multiphase image segmentation via Modica-Mortola phase transition, SIAM. J. Appl. Math., 67(2007), pp. 1213-1232.
[13] M. Kass, A. Witkin, and D. Tetzopoulos, Snakes: Active contour models, Int. J. Comput. Vision, 1(1988), pp. 321-331.
[14] C. Li C.-Y. Kao J.C. Gore and Z. Ding, Implicit active contours driven by local binaryfitting energy, CVPR07, 2007, pp. 1-7.
[15] J. Lie, M. Lysaker, X.-C. Tai, A binary level set model and some appplications to Mumford-Shah image segmentation, IEEE Trans. Image Process., 15(2006), pp. 1171-1181.
[16] J. Lie, M. Lysaker, X.-C. Tai, A variant of the level set method and applications to image segmentation. Math. Comp. 75(2006), PP. 1155–1174.
[17] B. Mory and R. Ardon, Fuzzy region competition: a convex two-phase segmentation framework, F. Sgallari, A. Murli, and N. Paragios (Eds.): SSVM 2007, LNCS 4485, pp. 214–226, 2007.
[18] D. Mumford and J. Shah, Optimal approximations by piecewise smooth functions and associated variational problems, Comm. on Pure and Applied Mathematics, 42(1989), pp. 577-685.
[19] N. Paragios and R. Deriche, Geodesic Active Regions for Supervised Texture Segmentation, Proceedings of International Conference on Computer Vision, 1999, pp. 22-25.
[20] C. Samson, L. B. Feraud, G. Aubert, and J. Zerubia, A level set model for image classification, Int. J. Comput. Vision, 40(2000), pp. 187-197.
[21] J. A. Sethian, Level set methods: evolving interfaces in geometry, fluid mechanics, computer vision and materials sciences (Cambridge, U.K., Cambridge Univ. Press), 1996.
[22] S. C. Zhu and A. Yuille, Region competition: Unifying snakes, region growing, and bayes/mdl for multiband image segmentation, IEEE Trans. Pattern Anal. Machine Intell., 18(1996), pp. 884-900.
[23] L. A. Vese and T. F. Chan, A multiphase level set framework for image segmentation using the Mumford and Shah Model, Int. J. Comput. Vision, 50(2002), pp. 271-293.
[24] J. Shen, A stochastic-variational model for soft Mumford-Shah segmentation, International Journal of Biomedical Imaging, Vol. 2006, Article ID 92329, pp. 1-14.